Spatial and temporal patterns of solar eclipses by Phobos on Mars

Bruce G. Bills
NASA Goddard Space Flight Center, Greenbelt, Maryland, USA

Scripps Institution of Oceanography, La Jolla, California, USA

Robert L. Comstock
Scripps Institution of Oceanography, La Jolla, California, USA

Received 5 November 2003; revised 14 October 2004; accepted 6 January 2005; published 7 April 2005.

[1] The spatial and temporal patterns associated with motion of the shadow of Phobos across the surface of Mars are quite different than those associated with solar eclipses on Earth. We present a simple analysis of variations in the position, velocity, size, and shape of the shadow. Simple expressions give reasonably accurate depictions of the shadow motion, which mainly consists of a subdiurnal longitude cycle and an annual latitude cycle. Over most of each year, there are an average of 3.22 shadow transits per day. The duration of the shadow transit depends on latitude. It is maximum at the equator and is then 11.8% of the orbital synodic period. As the subsolar point moves north, the shadow moves south, and vice versa. There is a narrow band, centered on the equator of Mars, within which every point is eclipsed at least once during each semiannual eclipse season. Outside that band, the density of coverage decreases slowly with increasing distance from the equator, until the limiting latitudes are reached. During epochs, like the present, when the obliquity of Mars is in excess of 21.2°, there are portions of each year during which no eclipses occur. As the obliquity increases beyond that transition value, the durations of the eclipse seasons decrease. The minimum possible eclipse season duration, expressed as a fraction of the Mars year, is the same as the maximum shadow transit duration, expressed as a fraction of the Phobos synodic period, since both ratios depend on the same geometry, which is essentially just the radius of the orbit of Phobos, compared to the radius of Mars.

Citation: Bills, B. G., and R. L. Comstock (2005), Spatial and temporal patterns of solar eclipses by Phobos on Mars, *J. Geophys. Res.*, *110*, E04004, doi:10.1029/2003JE002209.

> The Sun spins mindlessly overhead, the shadows lengthen and shorten as if by plan.
>
> John Gardner, *Grendel*

1. Introduction

[2] The shadows cast on the surface of Mars by its natural satellites, Phobos and Deimos, can provide information about relative positions of the Sun, Mars and the satellite casting the shadow. Accurately timed observations of these shadows by orbiting or landed spacecraft can provide positional information for the spacecraft. The durations and intensities of the shadows can act as probes of atmospheric conditions and subsurface thermal properties in the vicinity. Solar eclipse phenomena on Mars are sufficiently different from those on Earth that terrestrial eclipse experience is a poor guide. We present a simple analysis of the spatial and temporal patterns of eclipses on Mars and briefly comment on upcoming opportunities for observing these phenomena.

0148-0227/05/2003JE002209

[3] For solar eclipses on Earth, there is a quite extensive literature describing the basic phenomenology [*Zirker*, 1984; *Harrington*, 1997; *Maunder and Moore*, 1999; *Steel and Davies*, 2001], as well as applications to a wide range of solar [*Sykora et al.*, 2003; *Katsiyannis et al.*, 2003] and terrestrial phenomena [*Goodwin and Hobson*, 1978; *Bamford*, 2001]. Despite past use of the shadow of Phobos to probe thermal properties of the shallow subsurface of Mars [*Betts et al.*, 1995], and a recent suggestion of how it could be used to help locate a lander on the surface of Mars [*Christou*, 2002], we have been unable to find any general account of the behavior of eclipses on Mars, and have thus undertaken to produce a brief description of how the size, shape, and orientation of the shadow of Phobos varies with time, and how it moves across the surface of Mars.

[4] The frequency, intensity, and areal extent of solar eclipses are determined by the orbital parameters governing the geometry necessary to generate an eclipse. The relative motions of the primary and satellite determine eclipse frequency, while the physical dimensions of the satellite, and the radius of its orbit determine the properties of the shadow. The orbital conditions required for solar eclipses on

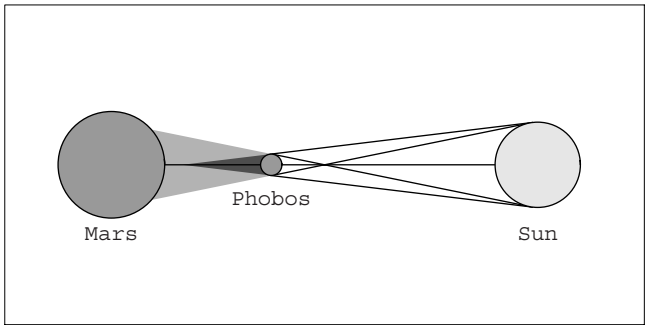

Figure 1. Shadow cone geometry. Within the umbral cone, with apex to the left of Phobos, the Sun is completely obscured. Within the penumbral cone, with apex to the right of Phobos, the Sun is only partially obscured. Since the umbral cone does not reach the surface of Mars at present, all eclipses there are partial.

Earth occur only rarely, with an average of 2.38 total and partial eclipses per year. At present, the lunar orbital radius is such that the apparent angular diameter of the Moon, as seen from Earth, approximates that of the solar disc. The lunar shadow consists of a dark, inner umbral cone, and a less dark outer penumbral cone. Eclipses occur when the lunar shadow cone intersects the surface of Earth. Total solar eclipses arise when the umbral cone reaches Earth's surface, and the Moon fully covers the Sun. However, total eclipses are infrequent due to the orbital alignments required for the umbral shadow to intersect Earth's surface. Partial eclipses are lower in intensity, but have vastly greater areal coverage than total eclipses making them more commonly observed than total eclipses.

[5] The size and orbital radius of Phobos are such that the umbral cone never reaches the surface of Mars, as is schematically illustrated in Figure 1. As a result, Mars never experiences total solar eclipses, but partial eclipses of the Sun by Phobos occur very often. The orbit of Phobos, with a mean radius of 2.76 Mars radii, negligible eccentricity, and small inclination, provides a favorable eclipse environment. Over much of each year, Mars averages 3.22 eclipses per day. In 1977, the Viking Lander (VL1) camera system observed 3 Phobos eclipse events, on 20, 24, and 28 September. On Earth, one would never see a series of eclipses at one location over such a short time scale. However, on Mars it is even possible to see two eclipses in one day at appropriate locations. One of the goals of the present study is to develop a simple model of the spatio-temporal patterns of eclipses with which we can address the likelihood of observing a sequence of eclipses, similar to that observed by Viking 1, at a single site.

[6] The size and shape of the shadow of Phobos on the surface of Mars, and the direction and speed of motion of that shadow across the surface all change over a range of time scales which are determined by the geometry of the orbits, and the rotation of Mars. As a result, the shadow geometry and motion vary with time of day, and time of year. On much longer time scales, the obliquity of Mars changes appreciably, and the orbit of Phobos is shrinking. These long period and secular trends also influence the eclipse phenomenology. Our main focus will be on the behavior at the present epoch, and we will only briefly consider the longer period trends, and mainly use them to illustrate properties of the present situation.

[7] Among the questions we will address in this study are: How does the size, and shape of the shadow change with time? What is the pattern of motion of the shadow? What fraction of the surface of Mars experiences an eclipse event over the course of a year? How do the spatial and temporal patterns vary with changing obliquity values?

[8] Our objectives are somewhat qualitative, and we seek to present a general overview of Mars eclipse phenomena. As a result, we apply a series of approximations that would be inappropriate for purposes requiring much greater numerical accuracy, such as predicting the actual time and place of eclipse events, or modeling light curves. In particular we assume circular orbits, with Phobos residing in the Mars equatorial plane, and treat Mars, Phobos, and the Sun as spheres. This does, of course, introduce some errors, but the general picture presented is essentially correct.

[9] Quite accurate models of the present motion of Phobos are available [*Jacobson et al.*, 1989; *Jacobson*, 1996; *Morley*, 1990; *Chapront-Touze*, 1990]. The long term tidal evolution is reasonably well understood [*Burns*, 1972, 1977, 1978; *Lambeck*, 1979; *Cazenave et al.*, 1980; *Szeto*, 1983; *Yokoyama*, 2002]. As Phobos is currently within the synchronous orbital distance, tides are transferring angular momentum from the orbit of Phobos to the spin of Mars, and the orbit is shrinking. On intermediate time scales of 10^4 to 10^6 years, the obliquity of Mars oscillates considerably [*Ward*, 1973, 1992; *Touma and Wisdom*, 1993; *Laskar and Robutel*, 1993] and that will influence the annual cycle of Phobos shadow latitudinal motions.

[10] The spatial and temporal patterns exhibited by the shadow of Phobos are somewhat complex, in detail, but much of this behavior can be understood as a superposition of several simpler components. We first consider the size and shape of the shadow. Next we examine patterns of motion of the shadow in longitude and latitude. Finally, we bring all these components together and examine the annual cycle of shadow coverage.

[11] The remainder of this paper is divided into five sections. In section 2, we describe the basic geometry and how that influences the size and shape of the shadow. In section 3, we examine the rapid longitudinal motion and annual latitudinal motion of the shadow, considering them first separately and then together. In section 4, we combine the position and size patterns to assess the annual pattern of shadow coverage. In section 5 we discuss possible applications of observations of the shadow of Phobos. In section 6, we briefly summarize the results.

2. Shadow Size and Shape

[12] In this section we begin an examination of the variations in size and shape of the shadow cast by Phobos on Mars. A simplifying feature of this aspect of the eclipse phenomenology at Mars is that the size and shape of the shadow each depend mainly on a single parameter, which is

the angular separation between the subsolar point and the center of the shadow.

2.1. Angular Size of Phobos

[13] Due to a well-known (but still poorly understood) optical illusion, the Moon appears larger when it is near the horizon than when it is near zenith. That appearance is misleading in two regards. In the first place, diurnal variations in lunar range from a surface point on Earth are small compared to monthly variations due to orbital eccentricity. In addition, the Moon is actually closer when it appears overhead than when it is on the horizon. Due to the smaller size of the orbit of Phobos, compared to the radius of Mars, this effect is much more pronounced at Mars than in the Earth-Moon system.

[14] The size of the shadow cast by Phobos is determined by the satellite's distance from the surface, and its physical dimensions. The figure of Phobos is well approximated by a triaxial ellipsoid with radii of

$$\{r_1, r_2, r_3\} = \{9.3, 11.1, 13.3\} \text{ km} \quad (1)$$

along axes oriented perpendicular to the orbit plane, along the velocity vector, and toward Mars, respectively [*Duxbury and Callahan*, 1989]. The semimajor axis of the orbit of Phobos is

$$a = 9380 \text{ km}. \quad (2)$$

As previously mentioned, we have assumed circular orbits for Mars and Phobos. From the surface of Mars, which we approximate as a sphere of radius R = 3390 km, the distance to Phobos varies substantially, depending on zenith angle ξ. The range r, from a point on the surface of Mars to the center of Phobos, is a function of the orbital radius a, Mars radius R, and the zenith angle ξ

$$r[\xi] = \sqrt{a^2 - R^2 \sin^2 \xi} - R \cos \xi. \quad (3)$$

The greatest distance to Phobos, from a point on the surface of Mars, occurs when Phobos is at the nadir of that surface point, and is thus quite invisible. Over the range of mutual visibility, the maximum range of 8746 km occurs when Phobos is on the horizon, and the shortest distance, 5990 km, occurs when Phobos is at the local zenith. Using the geometric mean of the two smaller radii (10.2 km) as a physical dimension, the angular radius of Phobos varies between a minimum of 0.067° at maximum distance, and a maximum of 0.097° at minimum distance.

[15] From the surface of Mars, at a mean distance of 1.524 AU, the Sun, with a radius of 6.96×10^5 km, subtends a disc with angular radius of 0.175°. As a result of the variations in the apparent diameter of Phobos, the solar area obscured by the Phobos disc as it transits the Sun ranges from a low of 12.1% during a transit near the horizon, to a high of 37.8% for a transit near zenith.

[16] Note that, as the distance from a point on the surface of Mars to Phobos increases, the angle subtended by Phobos decreases. However, due to the divergent nature of the penumbral cone, the size of the shadow increases with increasing distance.

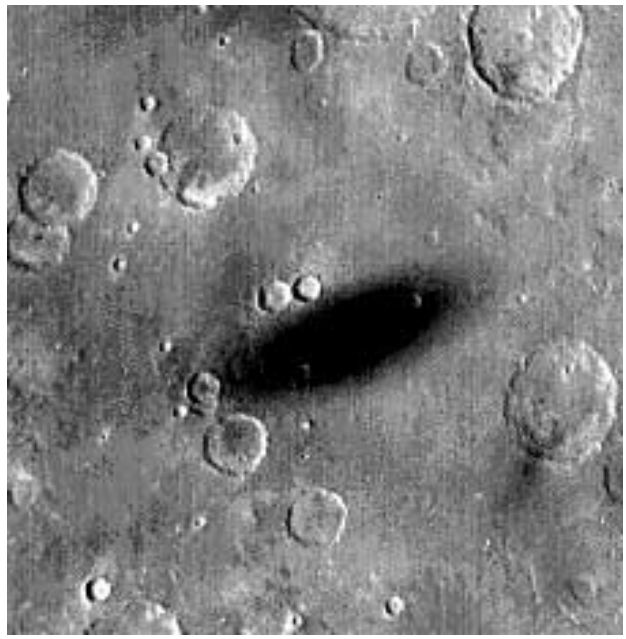

Figure 2. Phobos shadow image. This image was acquired by the Mars Observer Camera (MOC) on the Mars Global Surveyor (MGS) spacecraft on 26 August 1999.

2.2. Shadow Shape

[17] We now consider variations in the shape of the shadow. Many of the published images of the shadow of Phobos [*Betts et al.*, 1995] are quite elongated. Figure 2 shows a view of the shadow as seen on 26 August 1999 by the Mars Orbiter Camera (MOC) instrument on the Mars Global Surveyor (MGS) spacecraft. In that image, the shadow is roughly elliptical with a 3:1 aspect ratio. Is this degree of elongation of the shadow a common effect, and if so, how does it arise?

[18] Variations in the shape of the shadow of Phobos, if considered as a function of latitude, longitude, time of day and time of year, will be seen to be quite complicated. However, a change in perspective will prove quite helpful. At the level of approximation in which the orbits are considered to be circles and the bodies are spheres, the shadow shape depends only on a single parameter; the angular distance between the center of the shadow and the subsolar point.

[19] If we were to view Mars along the axis of the Phobos shadow cone, the shadow would appear very nearly circular. If, instead, we view the shadow from directly above its center, the shape of the shadow varies as it moves across the surface of Mars in the course of a single transit. If Phobos and Mars were both perfectly spherical, the outline of the shadow would be represented by the quartic curve which lies at the intersection of the spherical surface of Mars and the circular penumbral cone. If the cone axis contains the center of Mars, the shadow is a circle. As the cone axis moves away from the center of Mars, the shadow becomes roughly elliptical, with its long

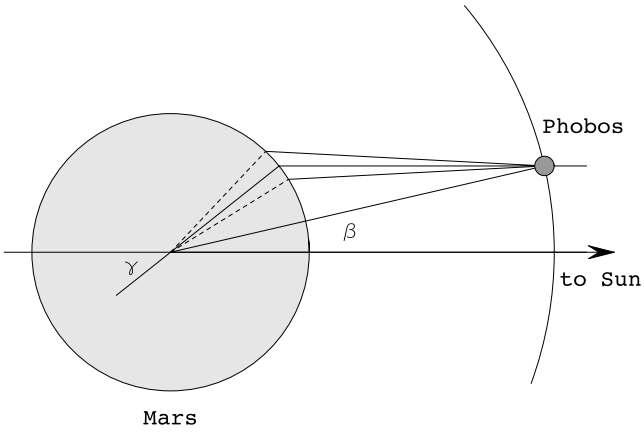

Figure 3. Shadow geometry relevant to shadow shape variations. The angle subtended at the center of Mars between Sun and Phobos is β; the angle between Sun and shadow is γ. The 3 closely spaced lines correspond to the principal points of the shadow. The center of the shadow is shown by a solid line, and the dashed lines indicate the limbmost point and the Sunmost point on the shadow perimeter.

axis along the great circle connecting the subsolar point to the center of the shadow.

[20] Figure 3 illustrates the position of Phobos and its shadow, as seen in a plane containing the Sun, the center of Mars, and Phobos. If the Mars-Sun line is taken to be the x axis, and the y axis is perpendicular to it, then the Cartesian coordinates of the center of Phobos are

$$x_p = a\cos\beta, \tag{4}$$

$$y_p = a\sin\beta, \tag{5}$$

where β is the angular separation between Sun and Phobos, as seen from the center of Mars. We consider the Cartesian coordinates of three points on the shadow: the center of the shadow, the point nearest the limb, and the point nearest the subsolar point. We will refer to them as the principal points of the shadow, and will use them to characterize the size and shape of the shadow. What we call here the center of the shadow is actually the shadow of the center of Phobos, though it will often be close to the geometric center of the shadow. We will examine the issue of asymmetry below.

[21] The coordinates of the shadow center are

$$x_c = R\cos\gamma_c = x_p - r_c, \tag{6}$$

$$y_c = R\sin\gamma_c = y_p, \tag{7}$$

where γ_c is the angular separation, as seen from the center of Mars, between the Sun and the shadow center, and r_c is the distance from Phobos to the shadow center. In similar fashion, the coordinates of the point on the shadow nearest the limb of Mars are

$$x_b = R\cos\gamma_b = x_p - r_b\cos\alpha, \tag{8}$$

$$y_b = R\sin\gamma_b = y_p + r_b\sin\alpha, \tag{9}$$

where r_b is the distance from Phobos to the shadow point nearest the limb and α is the shadow cone divergence angle. Likewise, and the coordinates of the point on the shadow nearest the subsolar point are

$$x_s = R\cos\gamma_s = x_p - r_s\cos\alpha, \tag{10}$$

$$y_s = R\sin\gamma_s = y_p - r_s\sin\alpha, \tag{11}$$

where r_s is the distance from Phobos to the shadow point nearest the subsolar point.

[22] These equations yield simple solutions for the variations in distance from Phobos and Mars-centered angles from the subsolar point to each of the principal points. For the center point we have

$$R\sin\gamma_c = a\sin\beta, \tag{12}$$

$$r_c = a\cos\beta - q_c, \tag{13}$$

with

$$q_c = R\cos\gamma_c = \sqrt{R^2 - a^2\sin^2\beta}. \tag{14}$$

The corresponding values for the limbmost shadow point are

$$R\cos\gamma_b = a\sin\alpha\sin(\alpha+\beta) + q_b\cos\alpha, \tag{15}$$

$$r_b = a\cos(\alpha+\beta) - q_b, \tag{16}$$

with

$$q_b = \sqrt{R^2 - a^2\sin^2(\alpha+\beta)}. \tag{17}$$

For the principal point nearest the subsolar point, the parameters are

$$R\cos\gamma_s = a\sin\alpha\sin(\alpha-\beta) + q_s\cos\alpha, \tag{18}$$

$$r_s = a\cos(\alpha-\beta) - q_s, \tag{19}$$

with

$$q_s = \sqrt{R^2 - a^2\sin^2(\alpha-\beta)}. \tag{20}$$

[23] The angular extent of the shadow along the short axis, or width, is now easy to estimate. Using the above results, we can write

$$R\sin\Delta\gamma_w = r_c\sin\alpha, \tag{21}$$

where $\Delta\gamma_w$ is the angular separation, as seen from the center of Mars, between the shadow center and either of the shadow edge points along the great circle perpendicular to the long axis.

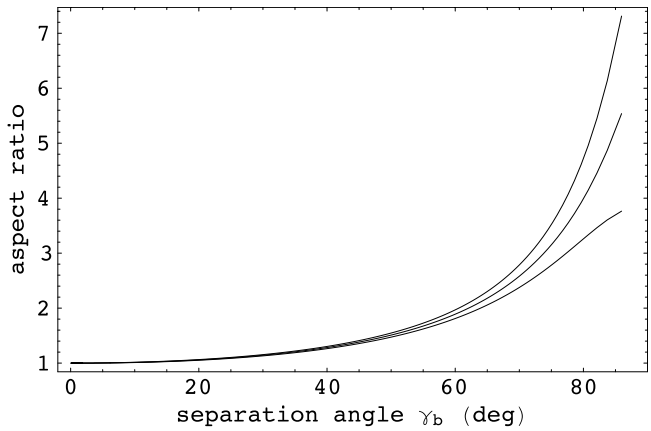

Figure 4. Variations in shadow aspect ratio. The central curve represents the average aspect ratio, or ratio of long axis to short axis lengths for the shadow of Phobos, and is shown as a function of γ_b, which is the angular separation between the subsolar point and the limbmost point on the shadow perimeter. The other two curves give the same ratio, but for the portions of the shadow which lie Sunward and limbward of the center.

[24] Using the angles defined above, the shape of the shadow of Phobos can be parameterized in terms of the aspect ratios of the Sunward and limbward portions as

$$h_s = \frac{\gamma_c - \gamma_s}{\Delta\gamma_w}, \tag{22}$$

$$h_b = \frac{\gamma_b - \gamma_c}{\Delta\gamma_w}, \tag{23}$$

and the overall shape can be parameterized in term of the aspect ratio of the complete shadow

$$h = \frac{1}{2}(h_b + h_s) = \frac{\gamma_b - \gamma_s}{2\ \Delta\gamma_w}. \tag{24}$$

Figure 4 illustrates the variations in these parameters as a function of γ_b which is the angular separation between the subsolar point and the limbmost point of the shadow of Phobos. Several features deserve comment. The shadow is circular at the subsolar point and becomes more elongated as it moves toward the limb. For small departures from circularity, the shadow is very nearly elliptical. As it becomes more elongated, it departs somewhat from the elliptical pattern and becomes somewhat asymmetric, with the center point closer to the subsolar principal point and farther from the limbmost principal point. As the shadow touches the limb, it has an aspect ratio of nearly 6:1. Of course, in this limit some of our approximations become problematic. In particular, the surface topography of Mars will severely distort the shadow as it approaches the limb. However, it is worth noting that the shadow is quite elongated much of the time.

[25] With this information, we now return to Figure 2, and attempt to understand the amount and direction of elongation of the shadow image. The aspect ratio of the shadow is roughly 3:1. This might appear, from Figure 4, to suggest that the center of the shadow is 60°–70° from the subsolar point. However, examination of shadows within craters suggests otherwise. In fact, the image was acquired at roughly 2 PM local time. The resolution of this dilemma is that MOC is a line-array or push-broom camera, and the image was acquired one row at a time. The MGS spacecraft was moving mainly in a north-south direction, while Phobos and its shadow were moving mainly in an east-west direction, but at a slower rate. This caused the image of a nearly circular shadow to appear quite elongated. In fact, the MOC wide angle camera has imaged the shadow of Phobos hundreds of times. The ratio of the synodic periods of Phobos and MGS is roughly 3.905, and the shadow is imaged roughly every 39th orbit of MGS, or every 10th orbit of Phobos. In all of those images, the shadow is elongated by the relative motion of the spacecraft and the shadow.

3. Shadow Motion

[26] We now turn our attention to the motion of the shadow across the surface of Mars. We will first examine the motions of Phobos and Sun across the sky, as seen from Mars. Next we consider the rapid longitudinal motions of the shadow, due to the orbital motions of Phobos and the rotation of Mars. After that, we consider the annual cycle of latitudinal shadow motion. Finally, we combine the two motions to generate a simple model of the latitudinal and longitudinal pattern of shadow paths across the surface of Mars.

3.1. Angular Rates of Sun and Phobos

[27] Motion of the shadow of Phobos depends on the relative motions, as seen from a point on Mars, between the Sun and Phobos. The angular speed of the Sun, as seen in a Mars fixed reference frame, is

$$s = n_m - \sigma_m, \tag{25}$$

where

$$n_m = 0.524033035 \text{ deg/day} \tag{26}$$

is the sidereal orbital mean motion of Mars, and

$$\sigma_m = 350.891983 \text{ deg/day} \tag{27}$$

is the sidereal spin rate of Mars. The resulting angular rate is

$$s = -350.367950 \text{ deg/day}. \tag{28}$$

The negative sign implies that the Sun rises in the east and sets in the west.

[28] The mean angular speed of Phobos, as seen in a reference frame rotating with Mars, and coincident with the center of Mars, is

$$p = n_p - \sigma_m, \tag{29}$$

where

$$n_p = 1128.8444155 \text{ deg/day} \tag{30}$$

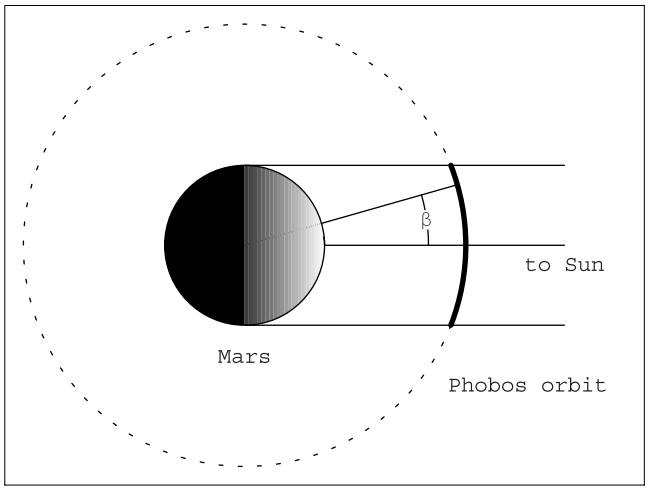

Figure 5. Longitudinal shadow motion. The heavy line along the orbit of Phobos indicates the portion of the orbit during which the shadow cone intersects the surface of Mars.

is the sidereal orbital mean motion of Phobos. The resulting mean rate is

$$p = 777.9524325 \text{ deg/day}. \tag{31}$$

The positive sign implies that Phobos rises in the west and sets in the east.

3.2. Subdiurnal Longitude Cycle

[29] The most rapid change in position of the shadow is that associated with the motion of Phobos around its orbit and the rotation of Mars. As a first approximation, suppose that the obliquity of Mars were zero. In that case, the motion of the shadow of Phobos would be extremely simple. The center of the shadow will always lie on the equator, and will move from west to east across the surface of Mars at a variable rate. The most rapid movement will be just as the shadow moves onto, or off of, the surface of Mars and will be slowest when the shadow crosses the location of local noon. The central meridian crossings are uniformly spaced in time, and occur at intervals of

$$\Delta t = \frac{2\pi}{n_p - n_m} = 0.319058 \text{ day}, \tag{32}$$

where n_p and n_m are the mean motions of Phobos and Mars, respectively.

[30] As shown in Figure 5, the beginning and end of a shadow transit correspond approximately to times when the angular separation β between the center of the solar disc and the center of the Phobos disc are such that

$$a \sin\beta = R. \tag{33}$$

As a result, the shadow transit duration δt comprises a fraction

$$\frac{\delta t}{\Delta t} = \frac{1}{\pi} \sin^{-1}\left(\frac{R}{a}\right) = 0.11785 \tag{34}$$

of the total orbit duration. If Mars were in synchronous rotation with the Sun, each shadow path would cover 180° of longitude. However, the more rapid rotation of Mars, at the rate σ_m, shortens the shadow path by the amount that Mars rotates, relative to the Sun, during the shadow transit, which amounts to 13.17°. In this simple case, a shadow stripe 166.83° long would occur every 7.66 hours. The centers of successive pairs of these stripes would be offset in longitude by

$$\Delta\phi = \Delta t(s_m - n_m) = 111.788^\circ. \tag{35}$$

As we will see subsequently, this simple model is a reasonably good approximation to the longitudinal motion of the shadow, even in the case of finite obliquity.

3.3. Annual Latitude Cycle

[31] We now consider the variations in latitude of the center point of the shadow over the annual cycle. Figure 6 illustrates the orientation of the orbit of Phobos, as seen from a perspective directly above the subsolar point, at 15 times uniformly spaced throughout the year. The latitude θ_s of the subsolar point on Mars changes throughout the year, and that influences the latitude of the shadow of Phobos. The annual cycle of subsolar latitude can be easily computed as a function of solar longitude L_s, which is measured from northern hemisphere vernal equinox, and the obliquity ε of Mars, or angular separation between spin pole and orbit pole. The relationship is

$$\sin\theta_s = \sin\varepsilon \sin(L_s), \tag{36}$$

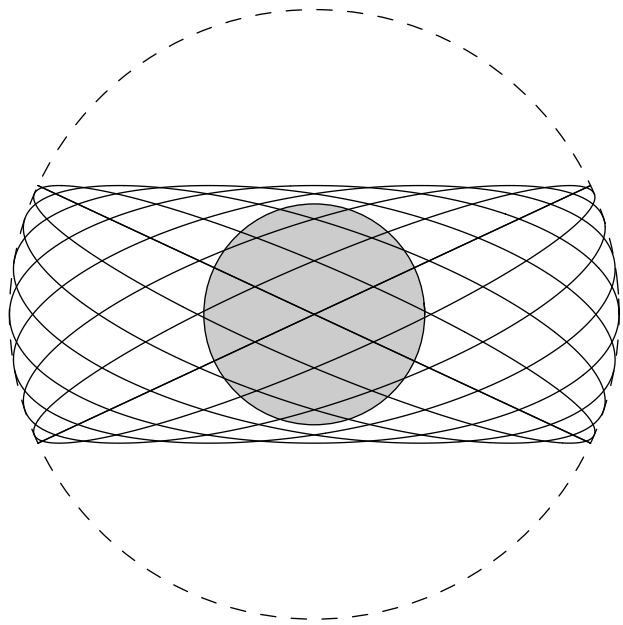

Figure 6. Views of Phobos orbit from the direction of the Sun. The gray disk represents Mars, and the elliptical curves represent the orbit of Phobos, as seen from a point directly above the sun-solar point, at 15 times uniformly spaced throughout the Mars year. Note that when viewed from some directions, the orbit does not project onto the surface of Mars.

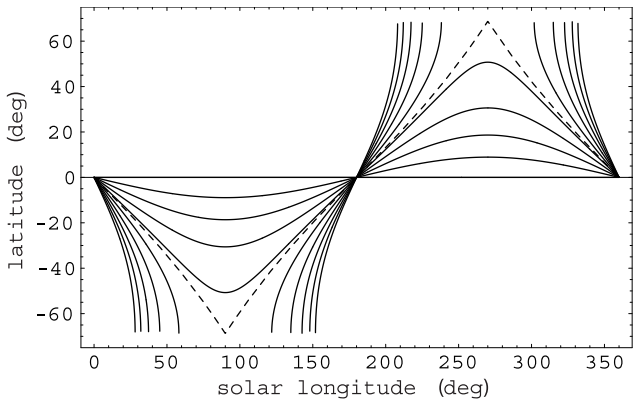

Figure 7. Latitudinal motion of shadow path centroid. The curves represent the annual cycle of variation in latitude of the shadow as it crosses the meridian containing the subsolar point, for different values of obliquity. The obliquity values range from 0 to 45°, in steps of 5°. The dashed line is for the transition obliquity of 21.21°, at which the shadow cone just passes poleward of the planet. At higher obliquities, there are gaps in the eclipse sequence.

where

$$\varepsilon = 25.2^\circ \tag{37}$$

is the current value of Mars obliquity.

[32] If we treat the Sun as though it were at infinite distance, then a necessary condition for an eclipse to occur at a specified point on the surface of Mars is that the distance of Phobos from the Mars-Sun line is equal to the distance of the surface point from that line. That condition will be met whenever

$$a \sin(\delta_p) = R \sin(\delta_m), \tag{38}$$

where a is the semimajor axis of the Phobos orbit, R is the mean radius of Mars, and the angles δ_p and δ_m are the Mars-centered distances from the Sun to Phobos and the surface point, respectively.

[33] If we make the approximation that Phobos lies in the equator plane of Mars, then

$$\delta_p = -\theta_s \tag{39}$$

and the latitude of the surface point is simply the difference between those angles

$$\theta_u = \delta_m - \delta_p. \tag{40}$$

Combining these results, we find that the latitude of the shadow center as it crosses the central meridian is a simple function of subsolar latitude and a fairly simple function of mean solar longitude:

$$\theta_u(L_s) = \theta_s(L_s) - \sin^{-1}\left[\frac{a}{R}\sin\theta_s(L_s)\right]. \tag{41}$$

Figure 7 illustrates this pattern. The obliquity value at which the center of the shadow path just passes off the planet at the summer and winter solstices is

$$\varepsilon_c = \arcsin\left(\frac{R}{a}\right) = 21.21^\circ. \tag{42}$$

For obliquity values less than this, each orbit of Phobos will generate a shadow transit across the surface. For obliquity values greater than ε_c there will be an extended length of time each year when there are no eclipse events.

[34] In this latter case, the annual pattern of eclipses will be characterized by two "eclipse seasons" when the Mars surface experiences an average of 3.22 eclipses per day, and two "no-eclipse seasons" when the orientation of the Phobos orbit is such that no point in the orbital track will generate a shadow that intersects the surface of Mars. The greater the obliquity value, in excess of the transition value, the longer the interval between eclipse seasons, as shown in Figure 7. At the present value of Mars obliquity, there is a 122 day time span between eclipse seasons twice per year, with the midpoints of the no-eclipse intervals occurring at the summer and winter solstices.

[35] If the obliquity were increased beyond the value at which "no-eclipse seasons" just begin, the duration of the eclipse seasons continues to diminish, but does not go to zero. The durations of eclipse seasons and the durations of individual shadow transits are both determined by the same basic geometry. As a result, the minimum duration of an eclipse season, expressed as a fraction of a year, is the same as the maximum duration of a single transit, expressed as a fraction of the Phobos orbital period. Both of those fractional durations depend only on the ratio of the orbital semimajor axis of Phobos to the radius of Mars, which is approximately 2.76.

3.4. Two-Dimensional Shadow Motion

[36] We now start an exploration of the full motion of the shadow of Phobos, in which the latitudinal and longitudinal cycles are coupled. In previous sections we have separately considered the fast longitudinal cycle and slow latitudinal cycle of shadow motion, exploiting the wide difference in time scales to approximate them as completely decoupled. If those motions were fully decoupled, the shadow path would be given by the superposition of the two cycles, with roughly 3.2 shadow transits per day, and the shadow path center point shifting steadily in longitude by 111.78° per transit, and the latitude of the center point following the annual cycle shown in Figure 7.

[37] There are two primary differences between the uncoupled and coupled cases. First is that the duration and longitudinal extent of the transits decreases as the subsolar point moves poleward. Second is that the limbmost edges of the transit paths curve away from the equator as the shadow moves poleward. In this section we will restrict our attention to the motion of the center of the shadow. In a subsequent section we will combine this motion with variations in the size, shape and orientation of the shadow itself.

[38] The path of the shadow across the surface of Mars can be derived from a simple model in which we follow the intersection of the Sun-Phobos line with a spherical Mars. If

Table 1. Fourier Series Representation of Discriminant Function

Index	Amplitude	Rate, deg/day	Period, day	Phase, deg	Source
0	−7.57726	0			
1	0.828711	1.04807	343.4898		$2\ n_m$
2	$1.8765\ 10^{-4}$	1128.32	0.319058		$n_p - n_m$
3	$9.3759\ 10^{-6}$	1129.37	0.389762		$n_p + n_m$
4	8.29307	2256.64	0.159529		$2(n_p - n_m)$
5	0.828711	2257.69	0.159455		$2\ n_p$
6	0.020703	2258.74	0.159381		$2(n_p + n_m)$

P and S are points at the centers of Phobos and the Sun, then a parametric equation representing the line through them is

$$Q = P + u\ (S - P), \tag{43}$$

where u is a parameter which specifies position along the line. When $u = 0$, the equation yields the position of Phobos, and when $u = 1$, it produces the position of the Sun. If we take the center of Mars to be our coordinate origin, and let the orbit plane of Mars define the x-y plane, then the intersection of the sphere of radius R with the line along the shadow axis is given by the condition

$$Q \cdot Q = R^2. \tag{44}$$

If this condition is written explicitly in terms of the parameter u, we obtain a quadratic equation of the form

$$a\ u^2 + b\ u + c = 0, \tag{45}$$

where

$$a = (S - P) \cdot (S - P), \tag{46}$$

$$b = 2\ P \cdot (S - P), \tag{47}$$

$$c = P \cdot P - R^2. \tag{48}$$

The discriminant of this equation is

$$d = b^2 - 4\,a\,c. \tag{49}$$

The value of this parameter tells a good deal about the geometry. There will be two solutions for the parameter u, and two corresponding points of intersection, if $d > 0$. The two intersection points are on opposite sides of Mars, and only one of them is shadowed by Phobos. If $d = 0$, there is a single solution, and a single intersection point. If $d < 0$, there are no real solutions to the equation, and no intersection. The condition for the line being tangent to the sphere, and thus marking the approximate beginning or end of a shadow transit is thus $d = 0$.

[39] If the discriminant is positive, then the Phobos-Sun line intersects the sphere at two points, corresponding to values of the line parameter

$$u = \frac{-b \pm \sqrt{d}}{2a}. \tag{50}$$

The shadow of Phobos will fall on the surface of Mars if, in addition, the Sun and Phobos are on the same side of Mars, so that

$$P \cdot S > 0. \tag{51}$$

In that case, the shadow is located at the point of intersection with the line which is given by the further conditions

$$P \cdot Q > 0, \tag{52}$$

$$S \cdot Q > 0, \tag{53}$$

which simply specify that both the Sun and Phobos are visible from the shadow point.

[40] Our next task is to obtain an explicit expression for the discriminant. If we denote rotation matrices

$$R_1[\alpha] = \begin{bmatrix} 1 & 0 & 0 \\ 0 & \cos\alpha & -\sin\alpha \\ 0 & \sin\alpha & \cos\alpha \end{bmatrix}, \tag{54}$$

$$R_3[\alpha] = \begin{bmatrix} \cos\alpha & -\sin\alpha & 0 \\ \sin\alpha & \cos\alpha & 0 \\ 0 & 0 & 1 \end{bmatrix}, \tag{55}$$

then the position of the Sun at time t will be given by

$$S[t] = a_m\ R_3[n_m\, t + \gamma_m] \cdot \{1, 0, 0\}^t, \tag{56}$$

where a_m and n_m are the semimajor axis and mean motion of the heliocentric orbit of Mars, and γ_m is a phase angle which specifies the position of Mars at the time origin. In a similar fashion, the position of Phobos is given by

$$P[t] = a_p\, R_3[\psi_m] \cdot R_1[\varepsilon_m] \cdot R_3\left[n_p\, t + \gamma_p\right] \cdot \{1, 0, 0\}^t, \tag{57}$$

where a_p, n_p and γ_p are the corresponding orbital parameters of Phobos, and ε_m is the obliquity of the spin pole of Mars and ψ_m is the corresponding azimuthal angle. If these values are substituted into the formula for the discriminant, it can be written in the form

$$d[t] = d_0 + \sum_{j=1}^{6} d_j \cos\left(s_j\ t + \gamma_j\right), \tag{58}$$

where the parameter values are listed in Table 1.

[41] Note that the six nonzero angular rates are easily separated into three groups. There are three rapid terms, with rates of $2(n_p - n_m, n_p, n_p + n_m)$ or roughly two cycles per Phobos orbit, two medium speed terms, with rates of $(n_p - n_m, n_p + n_m)$ or one cycle per Phobos orbit, and one slow term, with a rate of $2n_m$ or two cycles per Mars orbit. If the obliquity were zero, there would only be three angular rates, 0, $(n_p - n_m)$ and $2(n_p - n_m)$. A finite obliquity introduces splitting in the spectrum, with new frequencies offset by multiples of $2n_m$ from the original three. The side bands have smaller amplitudes.

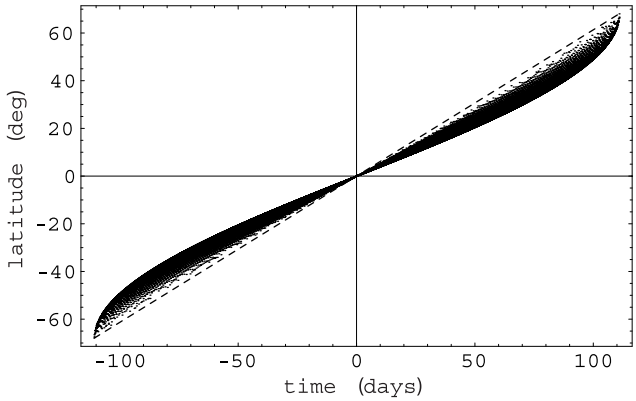

Figure 8. Latitudinal motion of shadow. This figure illustrates the pattern of motion of the center of the Phobos shadow over the course of a single eclipse season. Shadow center location computed at 60 second intervals for 240 days. At this scale a single shadow transit is essentially a vertical line.

[42] Having an explicit time dependence for the shadow axis discriminant function allows us to determine times at which the shadow axis moves onto and off of the surface of Mars. In order to obtain the trajectory across the surface of Mars of the shadow center point, we need to take two more basic steps. First, we solve for the Cartesian coordinates of the intersection point of the shadow axis with the sphere representing the surface of Mars. Then we convert from inertially referenced Cartesian coordinates to body-fixed polar coordinates.

[43] Figure 8 illustrates the latitude variations of the shadow center point over one complete eclipse season. It is a 222 day interval in which the shadow was moving from south to north, and the latitude was computed at 60 second intervals. At the scale of this image, each shadow transit is very nearly a vertical line. Note that the latitudinal extent of the shadow path is minimum at the equator and at the maximum poleward excursions.

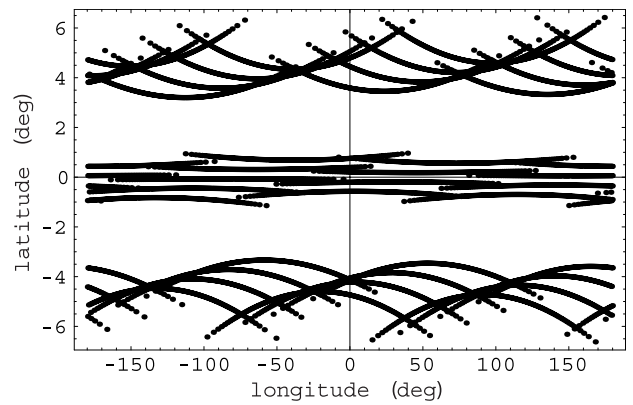

Figure 9. Shadow center motion. Each dot represents the location of the shadow center at a distinct time. The times represent 3 separate periods, each of 4 days duration, with 20 second sampling. The centers of the periods are separated by 10 days.

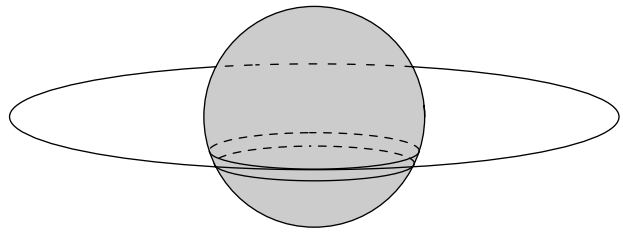

Figure 10. Source of shadow path curvature. The orbit of Phobos is seen from the direction of the Sun, along with the disc of Mars and lines of constant latitude. The latitude of the projection of the orbit onto Mars is different at the limb and the central meridian.

[44] Figure 9 illustrates the locations of the shadow center evaluated at 20 second intervals over 3 separate periods, each of 4 days duration, with 10 day offsets. The middle interval was chosen to coincide with equator crossing of the subsolar point. Note that, as shadow moves poleward, the shadow path becomes more curved away from the equator.

[45] The reason for that curvature is illustrated in Figure 10, which shows an orbit of Phobos, as seen from the direction of the Sun, along with lines of constant latitude which coincide with the projection of the orbit on the limb and the central meridian. As the orbit becomes more inclined to the Mars-Sun line, the latitudes at which the shadow path intersect the limb the central meridian diverge.

[46] Note that the model presented in this section has invoked several simplifying approximations. The main theme being circular orbits and spherical bodies. If a more accurate depiction of the trajectory of the center of the shadow were desired, the only modifications required would be replacing the simple orbits and planetary shape models with better versions. The basic idea of following the intersection point between the shadow cone axis and the planetary surface would need no fundamental change.

4. Shadow Coverage

[47] In this section we combine the previous simplified models of shadow size, shape, and centroid motion, and use them as building blocks to construct a model with which to address the full pattern of shadow coverage. One of the questions which motivated the present study is the following: how does the probability of seeing one or more eclipses during the course of a year depend on the location of the surface observer? In previous sections we have developed tools to track the shadow centroid, as it moves across the surface of Mars, but in order to address the coverage density question, we need to include the finite width and variable aspect ratio of the shadow.

[48] The axis defined by Phobos and the Sun determines the location of the shadow of the center of Phobos, which will be close to, but need not exactly coincide with, the center of the shadow. The lateral extent of the shadow can be computed by finding the intersection points between the spherical surface of Mars and the lines which generate the penumbral cone. As noted previously, the vertex of that cone is slightly Sunward of Phobos, but we will approxi-

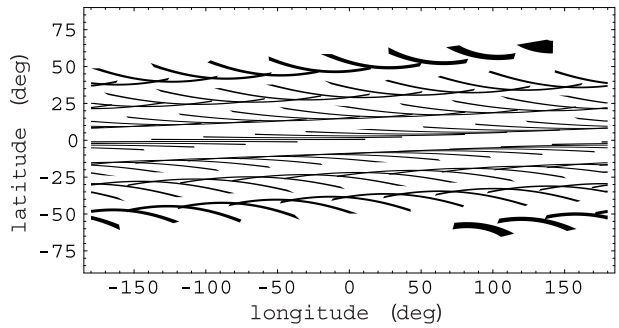

Figure 11. Partial shadow coverage during an eclipse season. Dark areas are regions of Mars covered by the shadow of Phobos when only including every 10th shadow transit. The partial coverage allows discrimination of the shapes and relative locations of separate transit events.

mate it as being located at the center of Phobos. To orient the shadow cone we define the following unit vectors:

$$\hat{e}_1 = \frac{S - P}{\| S - P \|}, \tag{59}$$

$$\hat{e}_2 = \frac{\hat{\mu} \times \hat{e}_1}{\| \hat{\mu} \times \hat{e}_1 \|}, \tag{60}$$

$$\hat{e}_3 = \frac{\hat{e}_1 \times \hat{e}_2}{\| \hat{e}_1 \times \hat{e}_2 \|}, \tag{61}$$

where S and P are the locations of Sun and Phobos, $\hat{\mu}$ is a unit vector along the spin pole of Mars, and

$$\| x \| = \sqrt{x \cdot x} \tag{62}$$

is the length of the vector x. The parametric equations for a circular cone can be written as

$$Q = q_1 \hat{e}_1 + q_2 \hat{e}_2 + q_3 \hat{e}_3, \tag{63}$$

with components

$$q_1 = u D, \tag{64}$$

$$q_2 = u D\, c \cos\theta, \tag{65}$$

$$q_3 = u D\, c \sin\theta, \tag{66}$$

where u is the generating parameter defining distance from the vertex,

$$D = \| S - P \| \tag{67}$$

is the distance between Sun and Phobos, c is the cone opening parameter, and θ is the azimuthal angle which spans the perimeter of the shadow as its value ranges from 0 to 2π. The cone opening parameter c is a function of the radii of the Sun and Phobos, and of the distance between them D:

$$c = \tan^{-1}\left(\frac{R_s + R_p}{D}\right). \tag{68}$$

[49] To find the location and shape of the shadow at a given time, we position Mars, Phobos and Sun at their respective locations, compute the intersections (if any) between a family of lines lying on the penumbral cone, parameterized by the azimuthal angle θ, and transform the coordinates of each intersection point from inertial Cartesian to Mars body-fixed latitude and longitude pairs.

[50] If the shadow is completely on the surface of Mars, then all values of θ will yield positive discriminant values and corresponding real valued Cartesian coordinates for the intersection points. If the shadow is only partly on Mars, then the outline of the shadow will have a truncated blunt end. Figure 11 illustrates a part of the coverage of Mars during a single eclipse season, with only every 10th eclipse shown, to better illustrate the individual path shapes and positions. During this season, the shadows were moving from north to south. Note that, as the shadow moves toward the equator, the shadow path becomes longer in longitudinal extent, narrower in latitudinal extent, and straighter.

[51] Figure 12 illustrates the complete pattern of coverage during the same eclipse season. Note that the fractional areal coverage is complete at low latitudes (less than 2 degrees from the equator), nearly uniform to quite high latitudes, and then drops quite quickly to zero at the limiting latitude. The locations of the mid-latitude gaps in coverage would be different during the following eclipse season, since the orbit period of Phobos and the rotation period of Mars are incommensurate. Figure 13 shows the same pattern, but viewed from the north pole.

[52] The total area covered at least once during an eclipse season is considerably less than the sum of the areas of the individual eclipses, since there is appreciable overlap. Even at the highest latitude to which eclipses extend, a point on the surface of Mars which experiences an eclipse has better than even odds of experiencing a second eclipse during the same eclipse season. As the rather uneven distribution of eclipses depends sensitively on the ratio of the orbital period of Phobos to the spin period of Mars, we can anticipate that this pattern will change appreciably as the orbit of Phobos

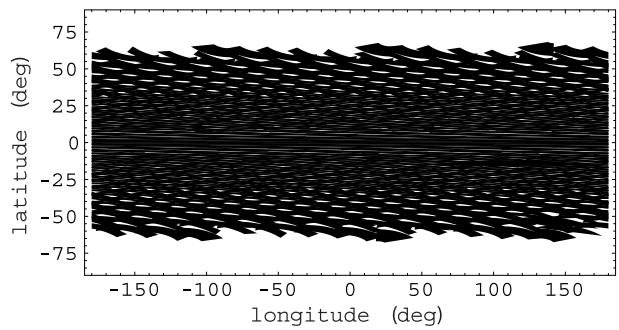

Figure 12. Complete shadow coverage during an eclipse season. Same as Figure 11, but showing aggregate coverage of all eclipses during a single eclipse season.

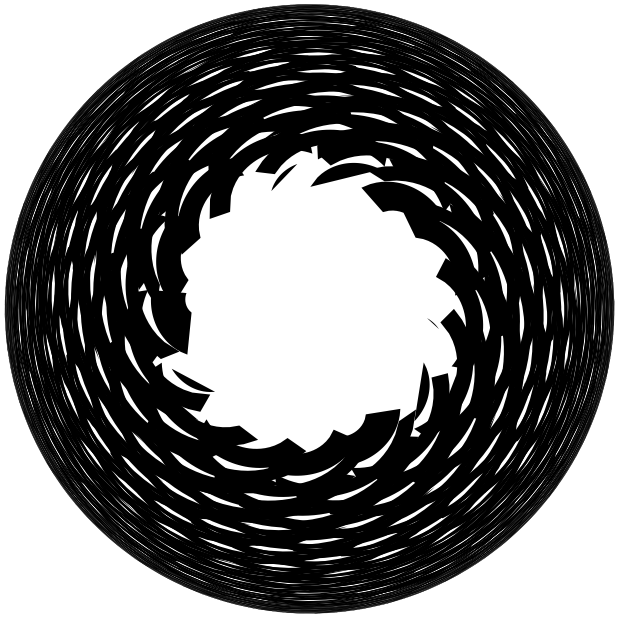

Figure 13. Polar view of shadow coverage. Same pattern as northern half of Figure 12, but viewed from above the north pole of Mars.

decays under tidal control. At present, the ratio of synodic periods is 3.22039. When the orbital mean motion of Phobos has increased to 1129.49°/day, and the synodic rate ratio has increased to 3.25, the central longitude of every fourth shadow transit will repeat. At that point in time, the areal coverage of shadows during a single eclipse season will look like Figure 14. The gaps in coverage are more regularly spaced than at present, but the total amount of coverage is not much different.

5. Applications

[53] Part of our motivation for examining the spatial and temporal patterns associated with the motion of the shadow of Phobos across the surface of Mars is that it is both interesting and potentially useful but has not, to our knowledge, been previously documented. Further justification is that familiarity with those patterns can be useful in planning for observations. Detailed planning of Phobos shadow observation programs would, of course, require accurate prediction of times and locations at which the shadow of Phobos will appear, and thus necessitate use of accurate models of the orbital motion. However, it is often difficult to extract from such strictly numerical models a general picture of the patterns of motion.

[54] One of the most obvious applications for observations of the shadow of Phobos is in determining positions. If the position of the observing platform is known, then the position of Phobos is constrained. If the observation point is not well known, then the time of a shadow observation will constrain the position of the observer. The latter strategy had been planned for the Beagle 2 lander [*Christou*, 2002]. The former strategy has been applied by the Spirit rover at Gusev crater [*Bell et al.*, 2004] and previously by the Viking Lander 1 in September of 1977 [*Jones et al.*, 1979; *Snyder*, 1979]. It is, in principle, possible to observe Phobos shadows from orbit with several different types of instruments. The Mars Observer Camera [*Malin et al.*, 1992] makes pole-to-pole scans of Mars in a wide angle viewing mode nearly every orbit [*Cantor et al.*, 2002]. Those images have serendipitously captured the shadow of Phobos dozens of times. The detector on the Mars Orbiter Laser Altimeter [*Zuber et al.*, 1992; *Abshire et al.*, 2000] views the surface of Mars in a narrow field of view, and has also captured 15 Phobos shadow events. Those sources of positioning information are presently being analyzed to better constrain the orbital motion of Phobos. It is also possible that other imaging systems, such as TES [*Christensen et al.*, 1992] and THEMIS [*Christensen et al.*, 2004] may have obtained useful positional constraints on the motion of Phobos.

[55] Another possible use of Phobos shadow observations is related to the brief thermal perturbation of the surface of Mars as the shadow passes by. This approach was exploited by *Betts et al.* [1995] to derive estimates of the thermal inertia of the upper few millimeters of the surface at several locations. The THEMIS and TES instruments may have captured images of the shadow which could be exploited in this way.

6. Summary

[56] In an attempt to understand the basic patterns of solar eclipses on Mars, we have developed and applied a suit of simple tools to describe the shape and motion of the shadow of Phobos as it moves across the surface of Mars. That motion is basically just a subdiurnal cycle of longitudinal motion and an annual cycle of latitudinal motion. The proximity of Phobos to Mars, and its location close to the equator plane ensures that eclipse are frequent. Over most of each year, there are an average of 3.22 shadow transits per day.

[57] The shape of the shadow is a simple function of distance from the subsolar point. When the shadow is near the subsolar point, it is very nearly circular. As it moves farther from the subsolar point, the shadow becomes

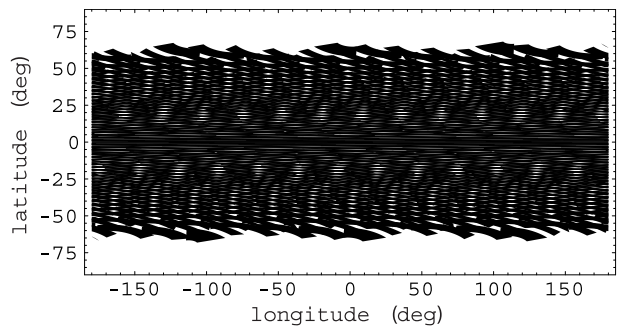

Figure 14. Shadow coverage at 13:4 synodic resonance. As Phobos approaches Mars, under tidal influence, the orbital period will decrease. When the ratio of synodic orbital period of Phobos to synodic rotation period of Mars is 3.25, the shadow pattern during a single eclipse season will be as shown. The longitude of the center of the shadow transit will repeat after 4 orbital periods, and the pattern will be somewhat more regular than at present.

elongated along the great circle which connects the subsolar point to the center of the shadow. Just before the shadow cone passes off the surface of Mars, the shadow outline is quite elongated.

[58] When the subsolar point is on the equator, the shadow path is also on the equator, and the area covered during the shadow transit has a nearly rectangular shape, approximately 167° in length and 0.5° in width, with slight widening at each end. As the subsolar point moves farther from the equator, the shadow band shortens in longitudinal extent, and curves away from the equator. As the subsolar point nears its maximum distance from the equator, the shadow cone passes poleward off the surface of Mars, and there is a season during which no eclipses occur.

[59] Within the latitudinal range over which eclipses are possible, they are fairly uniformly distributed. There is a narrow band, approximately 4° wide and centered on the equator, in which the coverage is complete. That is, during each eclipse season, every point within that region experiences at least one eclipse. Outside that band, the average density of shadow coverage decreases slowly with increasing distance from the equator.

[60] As the obliquity of Mars changes, the latitudinal extent of the shadow path changes considerably. During epochs when the obliquity is less than 21°, the eclipse season lasts all year. As the obliquity increases beyond that value, the durations of the eclipse seasons decrease.

[61] **Acknowledgment.** This work was partially supported by a grant from the NASA Mars Data Analysis Program.

References

Abshire, J. B., X. Sun, and R. S. Afzal (2000), Mars Orbiter Laser Altimeter: Receiver model and performance analysis, *Appl. Opt.*, *39*, 2449–2460.

Bamford, R. A. (2001), The effect of the 1999 total solar eclipse on the ionosphere, *Phys. Chem. Earth*, *26*, 373–377.

Bell, J. M., et al. (2004), Pancam multispectral imaging results from the Spirit Rover at Gusev crater, *Science*, *305*, 800–806.

Betts, B. H., B. C. Murray, and T. Svitek (1995), Thermal inertias in the upper millimeters of the Martian surface derived using Phobos shadow, *J. Geophys. Res.*, *100*, 5285–5296.

Burns, J. A. (1972), The dynamical characteristics of Phobos and Deimos, *Rev. Geophys.*, *10*, 462–483.

Burns, J. A. (1977), Orbital evolution, in *Planetary Satellites*, edited by J. A. Burns, pp. 113–156, Univ. of Ariz. Press, Tucson.

Burns, J. A. (1978), On the orbital evolution and origin of the Martian moons, *Vistas Astron.*, *22*, 193–210.

Cantor, B., M. Malin, and K. S. Edgett (2002), Multiyear Mars Orbiter Camera (MOC) observations of repeated Martian weather phenomena during the northern summer season, *J. Geophys. Res.*, *107*(E3), 5014, doi:10.1029/2001JE001588.

Cazenave, A., A. Dobrovolskis, and B. Lago (1980), Orbital history of the Martian satellites with inferences on their origin, *Icarus*, *44*, 730–744.

Chapront-Touze, M. (1990), Orbits of the Martian satellites from ESAPHO and ESADE theories, *Astron. Astrophys.*, *240*, 159–172.

Christensen, P. R., et al. (1992), Thermal Emission Spectrometer Experiment, *J. Geophys. Res.*, *97*, 7719–7734.

Christensen, P. R., et al. (2004), The Thermal Emission Imaging System (THEMIS) for the Mars 2001 Odyssey Mission, *Space Sci. Rev.*, *110*, 85–130.

Christou, A. A. (2002), Lander position determination on Mars using Phobos transits: Application to Beagle 2, *Planet. Space Sci.*, *50*, 781–788.

Duxbury, T. C., and J. D. Callahan (1989), Phobos and Deimos control networks, *Icarus*, *77*, 275–286.

Goodwin, G. L., and G. J. Hobson (1978), Atmospheric gravity waves generated during a solar eclipse, *Nature*, *275*, 109–111.

Harrington, P. S. (1997), *Eclipse!*, 280 pp., John Wiley, Hoboken, N. J.

Jacobson, R. A. (1996), The orbital motion of the Martian satellites: An application of artificial satellite theory, paper presented at AAS/AIAA Space Flight Mechanics Meeting, Am. Astron. Soc., Austin, Tex.

Jacobson, R. A., S. P. Synnott, and J. K. Campbell (1989), The orbits of the satellites of Mars from spacecraft and Earth-base observations, *Astron. Astrophys.*, *225*, 548–554.

Jones, K. L., R. E. Arvidson, E. A. Guiness, S. L. Bragg, S. D. Wall, C. E. Carlston, and D. G. Pidek (1979), One Mars year: Viking Lander imaging observations, *Science*, *204*, 799–806.

Katsiyannis, A. C., D. R. Williams, and R. T. J. McAteer (2003), Eclipse observations of high-frequency oscillations in active region coronal loops, *Astron. Astrophys.*, *406*, 709–714.

Lambeck, K. (1979), Orbital evolution of the Martian satellites, *J. Geophys. Res.*, *84*, 5651–5668.

Laskar, J., and P. Robutel (1993), The chaotic obliquity of the planets, *Nature*, *361*, 608–612.

Malin, M. C., G. E. Danielson, A. P. Ingersoll, H. Masursky, J. Veverka, M. A. Ravine, and T. A. Soulanille (1992), The Mars Observer Camera, *J. Geophys. Res.*, *97*, 7699–7718.

Maunder, M., and P. Moore (1999), *The Sun in Eclipse*, 282 pp., Springer, New York.

Morley, T. A. (1990), An improved analytical model for the orbital motion of the Martian satellites, *Astron. Astrophys.*, *228*, 260–274.

Snyder, C. W. (1979), The extended mission of Viking, *J. Geophys. Res.*, *84*, 7917–7933.

Steel, D., and P. Davies (2001), *Eclipse*, 492 pp., Joseph Henry, Washington, D. C.

Sykora, J., O. G. Dadalyan, and V. N. Obridko (2003), Connections between the white light eclipse corona and magnetic fields over the solar cycle, *Sol. Phys.*, *212*, 301–318.

Szeto, A. M. K. (1983), Orbital evolution and origin of the Martian satellites, *Icarus*, *55*, 133–168.

Touma, J., and J. Wisdom (1993), The chaotic obliquity of Mars, *Science*, *259*, 1294–1296.

Ward, W. R. (1973), Large scale variations in the obliquity of Mars, *Science*, *181*, 260–262.

Ward, W. R. (1992), Long-term orbital and spin dynamics of Mars, in *Mars*, edited by H. H. Kiefer et al., pp. 298–320, Univ. of Ariz. Press, Tucson.

Yokoyama, T. (2002), Possible effects of secular resonances in Phobos and Triton, *Planet. Space Sci.*, *50*, 63–77.

Zirker, J. B. (1984), *Total Eclipses of the Sun*, Van Nostrand Reinhold, Hoboken, N. J.

Zuber, M. T., D. E. Smith, S. C. Solomon, D. O. Muhleman, J. W. Head, J. B. Garvin, J. B. Abshire, and J. L. Bufton (1992), The Mars Observer Laser Altimeter investigation, *J. Geophys. Res.*, *97*, 7781–7797.

B. G. Bills and R. L. Comstock, Scripps Institution of Oceanography, La Jolla, CA 92093-0225, USA. (bbills@ucsd.edu)